Comparison of magnetic anisotropy and structural properties in chemically ordered CoPt and FePt nanoparticles

A. Tamion,[1,*] F. Tournus,[1] N. Blanc,[2] A. Hillion,[3] O. Proux ®,[4] A. Rogalev,[5] F. Wilhelm ®,[5] J. Gutiérrez Valdés ®,[6]
L. E. Díaz-Sánchez,[6] K. Sato,[7] G. M. Pastor ®,[8,†] and V. Dupuis ®[1]

[1]*Université Lyon 1, Centre national de la recherche scientifique (CNRS), Institut Lumière Matière Unité mixte de recherche (UMR) 5306,
69622 Villeurbanne, France*
[2]*Université Grenoble Alpes, CNRS, Grenoble INP, Institut Néel, 38000 Grenoble, France*
[3]*Université de Toulouse, Laboratoire de Physique et Chimie de Nano-Objets (LPCNO), Institut National des Sciences Appliquées
(INSA)-CNRS-Université Toulouse III - Paul Sabatier (UPS), 135 avenue de Rangueil, Toulouse 31077, France*
[4]*Observatoire des Sciences de l'Univers, 38051 Grenoble, France*
[5]*European Synchrotron Radiation Facility, BP 220, 38043 Grenoble, France*
[6]*Facultad de Ciencias, Universidad Autónoma del Estado de México, Instituto Literario No. 100. C. P. 50000 Toluca, Mexico*
[7]*Institute for Materials Research, Tohoku University, Sendai 980-8577, Japan*
[8]*Institut für Theoretische Physik, Universität Kassel, 34132 Kassel, Germany*

The intrinsic magnetic properties of nanoparticles (NPs) can be accurately determined using highly dispersed NPs in a matrix. In this paper, we study chemically ordered CoPt and FePt NPs with a diameter of 3 nm embedded in an amorphous carbon matrix. Although both alloys exhibit almost the same magnetic and crystallographic properties in the bulk materials, they are completely different as NPs. We show that their magnetic anisotropy differs greatly. To understand the origin of such a difference, a fine crystallographic structure study has been performed using extended x-ray absorption fine structure. In that respect, the atomic relaxations appear to be different in both nanoalloys. *Ab initio* calculations of the atomic relaxation shed light on these experimental results, showing that the wide distribution in Co sublattice should strongly alter the magnetic anisotropy of CoPt NPs.

I. INTRODUCTION

Magnetic nanoalloys are currently of great interest in a wide range of disciplines, including magnetic fluids, catalysis, biotechnology, biomedicine, magnetic resonance imaging, data storage, and environmental remediation [1–14]. To use magnetic nanoparticles (NPs) in any kind of application, it is necessary to know their magnetic properties, particularly their magnetic anisotropy energy. Otherwise, the small size of particles can be boon and bane since the magnetization direction of the NPs can rapidly switch due to thermal fluctuations, which is the so-called *superparamagnetic limit*. The blocking temperature T_B is the parameter used to separate the blocked (low temperature) and the superparamagnetic regime (high temperature). Here, T_B is directly proportional to the magnetic anisotropy energy ΔE which can be expressed in terms of the anisotropy constant K and the particle volume V through the well-known following relation: $T_B \approx \Delta E/25k_B$ with $\Delta E = KV$ [15].

In the bulk $L1_0$ phase, CoPt and FePt alloys exhibit similar magnetic and structural properties [16]. Indeed, the tetrago-

nalization of the unit cell as measured by the c/a ratio is almost the same ($c/a \approx 0.97$), and their uniaxial anisotropy constants are $K_{CoPt} = 5\,\mathrm{MJ\,m^{-3}}$ and $K_{FePt} = 7\,\mathrm{MJ\,m^{-3}}$ [17]. These extremely high uniaxial anisotropies are observed in the periodic solid due to the stacking of Co (or Fe) and Pt atomic planes along the (001) direction. In that respect, CoPt and FePt alloys in the chemically ordered $L1_0$ phase are some of the best candidates to reach a sufficiently high blocking temperature at the nanoscale and thus to be used in magnetic applications.

In this context, there has been considerable progress in the synthesis procedures of FePt [11,18] and CoPt [19–25] $L1_0$ NPs. Chemical ordering is often obtained by annealing, which goes with problems of pollution or coalescence. As a consequence, it is a very difficult task to ensure that chemically ordered NPs do not coalesce and do not interact with each other.

The main goals of this paper are then to determine and compare the intrinsic magnetic anisotropy constant of CoPt and FePt NPs and to understand the possible origin of any significant difference. For this purpose, we have elaborated similar samples made of chemically ordered NPs with negligible magnetic interactions. This paper is made up of six sections. After a section briefly describing the sample preparation and demonstrating the negligible magnetic interactions between NPs (Sec. II), we verify, using high-resolution

---

*alexandre.tamion@univ-lyon1.fr
†Present address: Research Center for Ultra-High Voltage Electron Microscopy, Osaka University, Ibaraki 567-0047, Japan.

transmission electron microscopy (HRTEM), the chemical ordering after annealing (Sec. III). In Sec. IV, the intrinsic magnetic properties of the NPs are accurately determined thanks to a global fit of various magnetic measurements.

The magnetic properties are then linked to the atomic structure using extended x-ray absorption fine structure (EXAFS) experiments and modeling in Sec. V. Finally, the major influence of atomic relaxations is inferred from *ab initio* calculations in Sec. VI.

II. SAMPLE PREPARATION

The alloy NPs are synthesized using the mass selected low-energy cluster beam deposition technique that allows us to grow thin films of preformed NPs deposited on a substrate [26,27]. In the following, we give a short description of this technique. Clusters are produced in a laser vaporization–gas condensation source. First, a plasma is created by the impact of a Nd : yttrium-aluminum-garnet laser beam focused on a CoPt or FePt rod and thermalized by injection of a continuous flow of helium at low pressure (typically 30 mbar) which induces the growth of the NPs. Second, the NPs are stabilized and cooled down in the supersonic expansion which takes place at the exit nozzle of the source. NPs are mass selected by an electrostatic quadrupole and transferred to an ultrahigh vacuum chamber (base pressure of 10^{-10} mbar) where they are deposited at low kinetic energy together with carbon atoms onto a carbon buffer.

In this physical process, the mean cluster composition is directly the rod composition. The distribution of composition is only statistical and depends on the number of atoms per cluster; *a priori* the low composition dispersion is the same in both CoPt and FePt NPs [28–31]. Even if in FePt NPs prepared by the chemical way the $L1_0$ order cannot be achieved for particles <3 nm [32], by the physical way, the $L1_0$ chemical order has been observed in particles with a diameter $\sim$2 nm [28,33,34]. Both two-dimensional (2D) transmission electron microscopy (TEM) grids and three-dimensional (3D) diluted samples have been prepared. The 3D samples used in magnetometry and EXAFS measurements have a concentration of only 0.5% vol. to avoid coalescence and to keep the magnetic interactions negligible. Copper grids coated by a thin amorphous-carbon layer for TEM and HRTEM observations and silicon substrates for magnetic measurements have been used.

A. Size distribution

The probability density function (PDF) of the diameter of mass-selected clusters follows a Gaussian distribution [35,36]. In the present case, PDFs of the incident CoPt and FePt clusters have been deduced from TEM observations. The mean diameters of the NPs are $D_{CoPt} = 3.2$ nm and $D_{FePt} = 3.4$ nm with a relative standard deviation $\sigma_D/D = 0.08$ for both CoPt and FePt NPs. Let us remind the reader that as-prepared NPs are in the $A1$ chemically disordered phase [28]. To promote the chemically $L1_0$ ordered phase, the samples must be annealed at 600 °C for 2 h.

B. Magnetic interactions

All magnetic measurements have been performed in a commercial superconducting quantum interference device magnetometer (Quantum Design MPMS 5XL) at various temperatures. Isothermal remanent magnetization (IRM) together with direct-current demagnetization (DcD) curves at low temperature have been used to detect the magnetic interactions between NPs [37,38].

In the IRM(H) measurement, the NP assembly is demagnetized by zero field cooling (ZFC) from the superparamagnetic regime. Then a magnetic field H is applied and removed: We acquire the IRM moment. By successively increasing H and removing it, we finally obtain a full IRM(H) curve. The maximum of the IRM(H) curve is the remanent magnetic moment m_R also measured in the hysteresis loop. In the DcD(H) measurement, the process is the same; the only difference comes from the initial state which is m_R [the maximum of the IRM(H)]. These two kinds of measurements, where the only difference is then the initial magnetic configuration, probe the irreversible magnetization switching [39], which means that there is no effect of superparamagnetic particles, diamagnetic substrate, or paramagnetic impurities, for instance. Moreover, IRM(H) and DcD(H) are also used to characterize the nature of interactions via the well-known parameter $\Delta m = \text{DcD}(H) - [m_R - 2\,\text{IRM}(H)]$. This parameter should be close to zero when interparticle interactions are negligible [37,38,40–42]. The IRM, DcD, and Δm curves for CoPt and FePt NP assemblies are given in Fig. 1 before and after annealing. There is no detectable magnetizing ($\Delta m > 0$) or demagnetizing ($\Delta m < 0$) interactions in as-prepared and annealed nanomagnets, showing that clusters remain well separated inside the matrix even after annealing.

III. CHEMICAL ORDERING

The samples are characterized by HRTEM. In addition to a JEOL 2010F microscope (operating at 200 kV and with a field emission gun), we have used an FEI Titan 80-300 microscope operating at 300 kV with a field emission gun and a Cs corrector for the objective lens. This yields HRTEM images with highly improved spatial resolution [43]. Both for annealed FePt and CoPt, we observe NPs with a single chemically ordered domain all along the NP [see Figs. 2(a) and 2(c)].

These monodomain NPs will be referred to as mono-$L1_0$ particles in the following sections. The chemical order parameter (S) of mono-$L1_0$ CoPt particles, with a diameter $\sim$3 nm, has been previously evaluated by HRTEM and simulations ($S \in [0.85, 1]$) [44].

We also observe chemical order in particles consisting of more than one crystalline domain. As an example, we can observe in Fig. 2(b) a CoPt NP where the $L1_0$ order is clearly visible on top with a $L1_0$ domain (where d_{001} is shown) which does not extend to the entire particle. However, the zone where d_{110} is shown is also chemically ordered but along a different direction.

Here, (111) twins, as displayed in Fig. 2(d), can lead to the observation of different orientations of $L1_0$ chemical order. We also observe decahedral particles, made of five $L1_0$
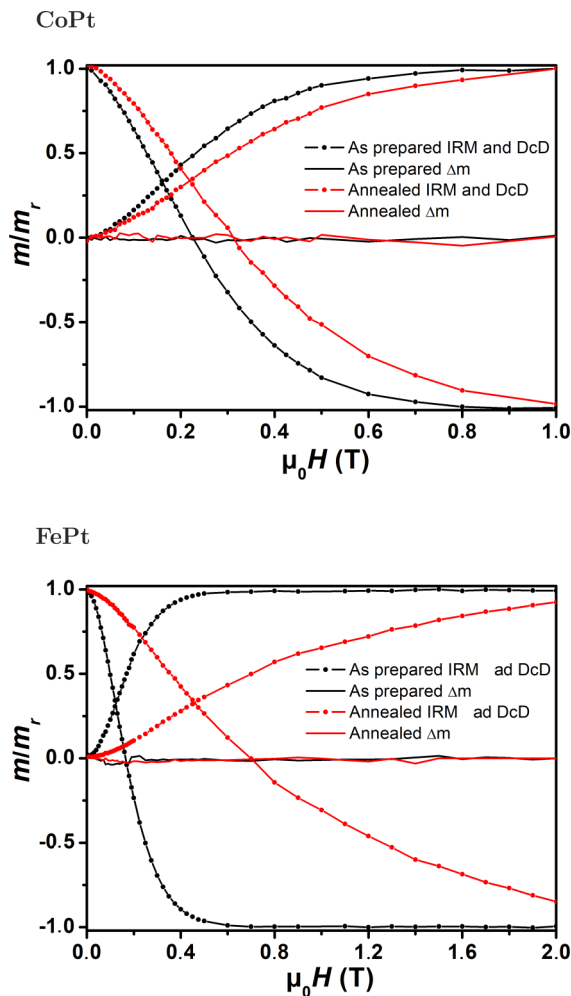
FIG. 1. Isothermal remanent magnetization (IRM)(H), direct-current demagnetization (DcD)(H), and Δm performed at $T = 2$ K of the CoPt and FePt samples before and after annealing.
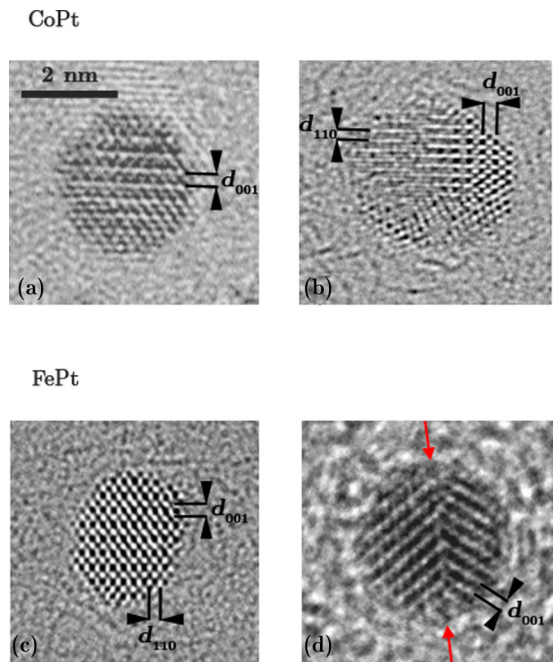

FIG. 2. High-resolution transmission electron microscopy (HRTEM) images of $L1_0$ (a) monodomain and (b) multidomain CoPt particles. HRTEM images of an $L1_0$ (c) monodomain FePt particle and (d) an FePt particle exhibiting two $L1_0$ domains joined by a (111) twin. Note that the (001) and (110) periodicities are the signatures of $L1_0$ chemical order.

domains joined by a (111) twin, and even icosahedral particles. Several theoretical investigations have predicted, for NPs <3 nm, the stability of these exotic structures displaying at the same time a fivefold symmetry and a chemical order [45–47].

All these particles, which are chemically ordered but with two or more $L1_0$ domain orientations, will be refereed to as multi-$L1_0$ in the following sections. More information about the chemical ordering of such NPs can be found in Ref. [33].

The statistical abundance of each type of structure cannot be determined precisely using HRTEM [33]. Nevertheless, we can observe mono-$L1_0$ particles in both CoPt and FePt nanoalloys. From a magnetic point of view, it is expected that the uniaxial magnetic anisotropy of multidomain decahedral, icosahedral, or twinned particles, despite the fact that they are all composed of ordered domains, will be lower than the uniaxial magnetic anisotropy of mono-$L1_0$ domain particles. In fact, locally, the orientation of the easy and hard axes within each domain should be different. We can then anticipate at least two different magnetic behaviors in such samples composed of chemically ordered NPs, the first one due to the mono-$L1_0$ NPs and the second one due to the multi-$L1_0$ NPs. In addition, we expect a significant anisotropy constant

dispersion reflecting the variety of atomic arrangements in NPs [29].

IV. MAGNETIC PROPERTIES

The high-temperature ($T = 300$ K) and low-temperature ($T = 2$ K) magnetization loops, ZFC/field cooling (FC) susceptibility curves, as well as the IRM (2 K) curve are shown in Fig. 3 for CoPt and FePt clusters before and after annealing. All the ZFC/FC curves display the characteristic behavior of an assembly of magnetic NPs, namely, a crossover between the blocked regime and the superparamagnetic regime.

At first glance, and for the as-prepared samples [Figs. 3(a) and 3(c)], all the magnetic curves appear very similar for CoPt and FePt NPs. The magnetic characteristics of these face-centered cubic (fcc) $A1$ clusters [28] seem to be almost the same, irrespective of chemical composition. After chemical ordering, the magnetic properties of CoPt NPs display a moderate change [Fig. 3(b) compared with Fig. 3(a)]. The temperature corresponding to the maximum of the ZFC curves increases, as already observed in CoPt NPs with a larger size dispersion [28]. In contrast, for FePt clusters, the magnetic behavior drastically changes upon annealing [see Figs. 3(c) and 3(d), note that the axis scales are different]. The shape of the ZFC/FC curves [Fig. 3(d)] indicates the presence of a large distribution of magnetic anisotropy energies, as the splitting temperature between ZFC and FC is very high (180 K) compared with the maximum of the ZFC ($T_{max} = 60$ K).

A more quantitative analysis is possible thanks to a previously developed theoretical framework enabling a global
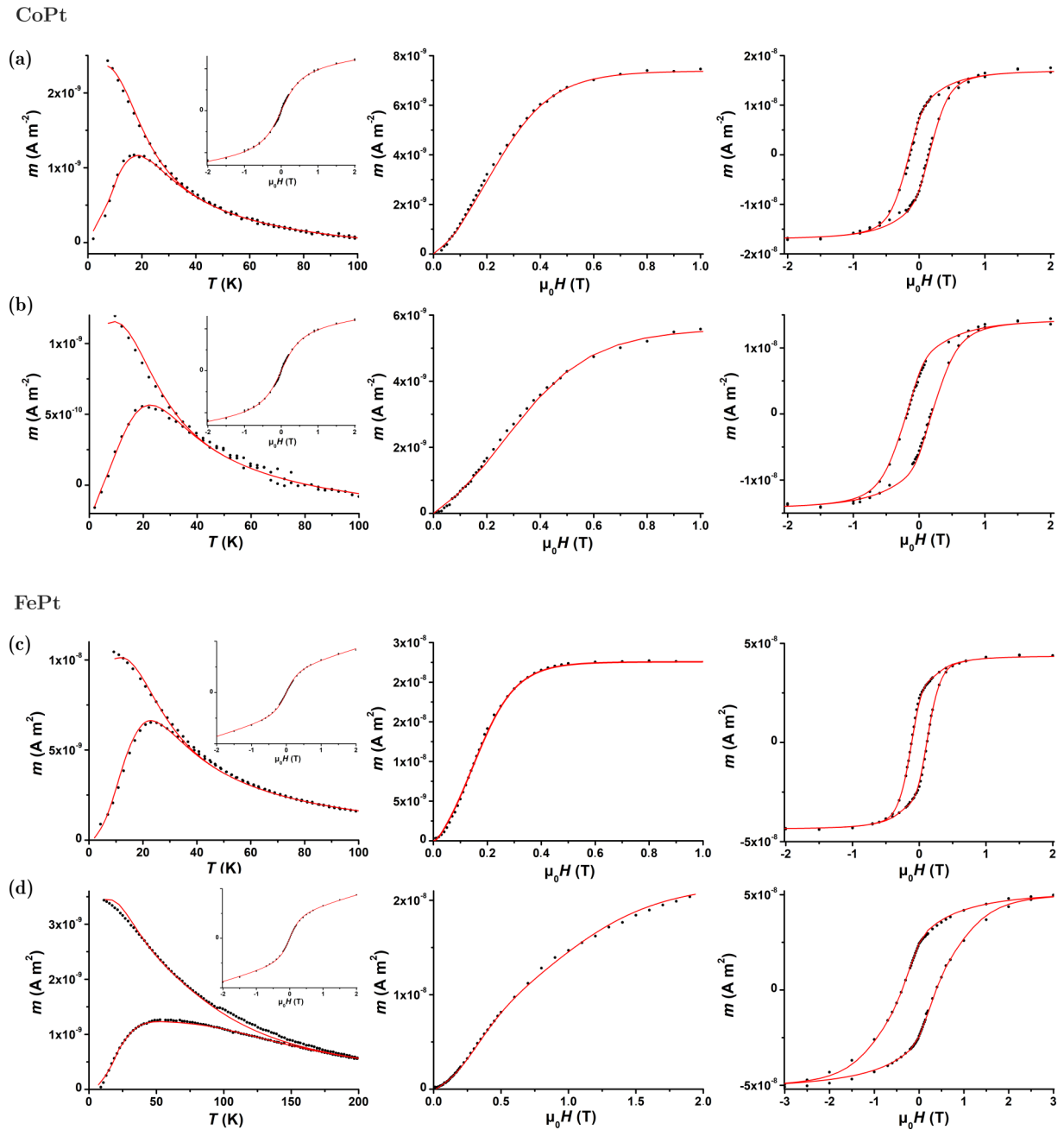
CoPt

FePt

FIG. 3. Experimental (black dots) and simulated (red solid lines) zero field cooled (ZFC)/field cooled (FC) curves, superparamagnetic magnetization loop at 300 K (in inset), isothermal remanent magnetization (IRM) curve, and hysteresis loop at 2 K, for (a) and (b) CoPt and (c) and (d) FePt clusters (a) and (c) before annealing and (b) and (d) after annealing. Considering a second-order anisotropy term K_2 and a distribution of anisotropy constant K_1 is necessary to accurately simulate all the curves. Note that the horizontal scales are different for annealed FePt clusters in (d).

fitting procedure of the entire set of magnetic measurements [48–51]. In this way, the magnetic measurements can be reproduced with a limited number of parameters which describe the nanomagnets regarded as noninteracting macrospins. These are the magnetic size distribution (Gaussian with an average diameter D and a standard deviation σ), the first-order anisotropy constant distribution (assumed to be Gaussian [50] with an average anisotropy constant $\overline{K_1}$ and a standard deviation σ_{K_1}), and the biaxial anisotropy ratio K_2/K_1. Such a biaxial description is used

to reflect the nonideal morphology of the NPs [49,52]. The actual global fits are presented in Fig. 3 for each sample by the red solid curves. The corresponding fitting parameters are summarized in Table I.

The chemically disordered CoPt and FePt $A1$ NPs exhibit identical magnetic properties within the experimental uncertainty. The mean anisotropy constant $\overline{K_1}$ and the K_2/K_1 ratio are almost the same as those measured in pure fcc Co NPs [53]. In fact, both CoPt and FePt $A1$ NPs behave like fcc Co particles, where the biaxial contribution and the value

TABLE I. For each sample, the ZFC peak temperature ($T_{\max}$), low-temperature coercivity ($\mu_0 H_c$), median magnetic diameter (D) and dispersion parameter (σ) of the Gaussian particle size distribution, median anisotropy constant (K_1) and standard deviation (σ_{K_1}) of the anisotropy constant distribution, and biaxial anisotropy ratio K_2/K_1 determined by a global fit of the ZFC/FC susceptibility curves, low-temperature IRM curve, and $m(H)$ loops at 2 and 300 K. The clusters magnetizations have been deduced from XMCD measurements [31], i.e., 10^6 and 1.28×10^6 A m^{-1}, respectively, for CoPt and FePt clusters.

Sample	$T_{\max}$(K)	$\mu_0 H_c$(mT)	D(nm)	σ/D	$\overline{K}_1$(kJ/m^3)	$\sigma_{K_1}/\overline{K}_1$	K_2/K_1
As-prepared CoPt	19	0.13	3.2 ± 0.2	0.10 ± 0.02	200 ± 20	0.44 ± 0.15	1.2 ± 0.2
Annealed CoPt	22	0.18	3.2 ± 0.2	0.10 ± 0.02	330 ± 30	0.47 ± 0.15	1.2 ± 0.2
As-prepared FePt	22	0.12	3.5 ± 0.2	0.10 ± 0.02	210 ± 20	0.32 ± 0.15	1.0 ± 0.2
Annealed FePt	55	0.37	3.5 ± 0.2	0.10 ± 0.02	400 ± 40	0.35 ± 0.15	1.0 ± 0.2
					1100 ± 150	0.35 ± 0.15	0.3 ± 0.2

of K_1 can be explained by the presence of additional or incomplete facets at the surface of the particles [51,54–56]. This shows that, before annealing, the magnetic anisotropy of the chemically disordered particles is dominated by the shape and the surface structure.

Let us remind the reader that, after annealing, HRTEM study has previously shown monodomain $L1_0$ (mono-$L1_0$) NPs and multidomain $L1_0$ (multi-$L1_0$) NPs in both CoPt and FePt alloys.

First, we will discuss the magnetic properties of FePt NPs after annealing and then the annealed CoPt NPs. For the annealed FePt NPs, we use a bimodal anisotropy constant distribution to accurately reproduce the experimental curves (Table I and Fig. 4 where two peaks are present). If we use only one large anisotropy constant distribution (Gaussian or log-normal), some important points of the curves (the merging point between the ZFC and FC or narrowing of the hysteresis loop at $m = 0$) are not well reproduced. The simplest distribution which allows us to perform a satisfactory fit is a bimodal Gaussian anisotropy constant distribution.

Motivated by the HRTEM observations of both monodomain (mono-$L1_0$) and multidomain (multi-$L1_0$) FePt NPs, we consider that each of these types of structures should have its own anisotropy constant distribution. Then the mean anisotropy constant of the multi-$L1_0$ FePt NPs is $\sim$400 kJ m^{-3}, whereas mono-$L1_0$ FePt NPs exhibit a strong mean anisotropy constant $\sim$1.1 MJ m^{-3}.
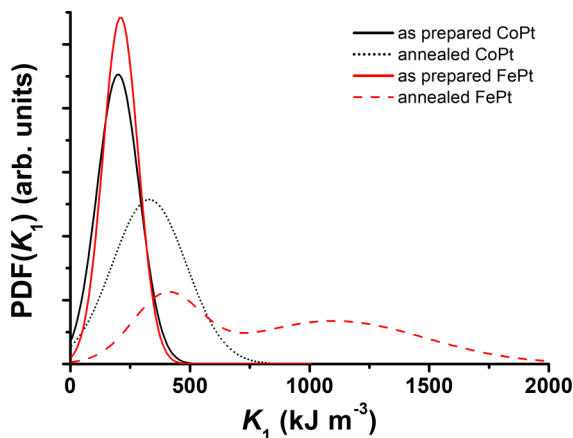

FIG. 4. Magnetic anisotropy distribution of the as-prepared and annealed particles, as deduced from magnetic measurement fits.

Note that 30% of the FePt NPs exhibit an anisotropy constant (K_1) >1 MJ m^{-3}, and the switching field of some $L1_0$ FePt clusters is >2 T [Fig. 3(d)]. In addition, the K_2/K_1 ratio is lower for the FePt mono-$L1_0$ NPs ($K_2/K_1 = 0.3$). This feature suggests that, for the FePt mono-$L1_0$ NPs, the principal contribution to the magnetic anisotropy energy comes from the $L1_0$ stacking (shape and faceting lead to a biaxial anisotropy [51,52,54,55]).

After annealing, and as previously shown using different annealing temperatures [28,57], the CoPt magnetic anisotropy slightly increases, which is visible as $T_{\max}$ and $\mu_0 H_c$ enhancements (Fig. 3). This feature is attributed to the chemical ordering. The K_2/K_1 ratio is almost the same (Table I), which suggests that the magnetic anisotropy still reflects the surface contributions. However, the most important difference between annealed CoPt and FePt NPs is that only one Gaussian anisotropy constant distribution is necessary to reproduce all the magnetic measurements performed on the annealed CoPt NPs (see Fig. 4). These features indicate that magnetic anisotropy constants of mono-$L1_0$ and multi-$L1_0$ CoPt clusters are similar. In all the magnetic measurements, there is no sign of a high magnetic anisotropy in chemically ordered CoPt NPs.

As already mentioned, in bulk material, the anisotropy constant is 5 and 7 MJ m^{-3} [17] (and references therein), respectively, for CoPt and FePt $L1_0$ alloys. Even for the mono-$L1_0$ FePt NPs, the magnetic anisotropy ($K_1 = 1.1$ MJ m^{-3}) is reduced compared with the bulk. Some theoretical studies performed on perfect CoPt and FePt $L1_0$ NPs have shown that, for small sizes, the magnetic anisotropy constant should slightly decrease [58–60]. In fact, cluster surface breaks the $L1_0$ periodicity which implies a decrease of the uniaxial magnetic anisotropy.

Finally, the determination of the magnetic properties leads to a major question: Why is the magnetic anisotropy magnitude comparable in multi-$L1_0$ and mono-$L1_0$ CoPt NPs, whereas it is possible to distinguish two different magnetic behaviors in FePt?

V. ATOMIC FINE STRUCTURE

To answer these questions, we have performed EXAFS measurements on the annealed CoPt and FePt particles. X-ray absorption spectroscopy (XAS) at the Co-K, Fe-K, and Pt-L edges has been performed at room temperature on the CRG BM30b-FAME [61] and ID12 beamlines [62] of the European
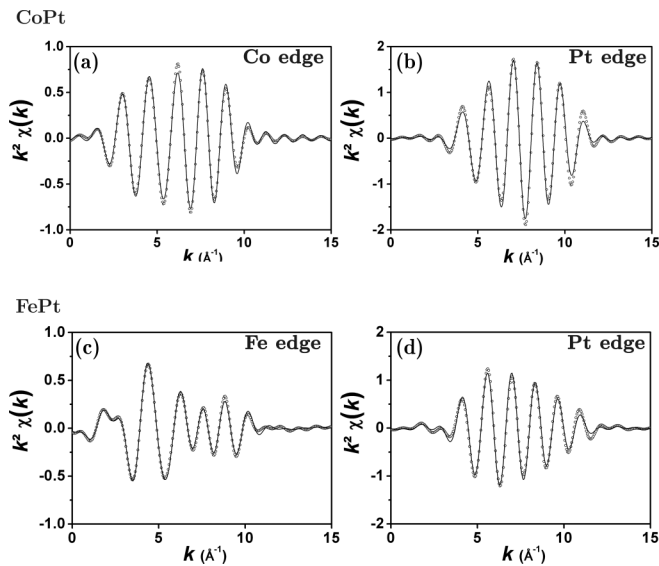
CoPt

FePt

FIG. 5. Comparison between the experimental extended x-ray absorption fine structure (EXAFS) signal [dots, contribution of the nearest-neighbor (NN) peak only] and simulated curves (solid lines) at the (a) Co-*K* edge, (b) Pt-*L* edge, (c) Fe-*K* edge, and (d) obtained on the chemically ordered CoPt and FePt particles.

Synchrotron Radiation Facility. A quantitative EXAFS analysis is performed by fitting the k^2-weighted function $\chi(k)$ to the standard EXAFS formula, using ARTEMIS software [63] and focusing on the nearest-neighbor (NN) contribution. Debye-Waller (DW) parameters are used to account for bond-length dispersion. The edge energy is allowed to slightly vary for the different samples but is taken to be the same for the Pt, Co, and Fe neighboring shells. The experimental and adjusted curves are presented in Fig. 5, and the best fit values are summarized in Table II.

A transition metal (TM) atom is surrounded by N_{TM} atoms at a distance d_{TMTM} and N_{Pt} platinum atoms at a distance d_{TMPt}. As expected from the HRTEM observations, the ratios $N_{Pt}/N_{TM} = 2$ at the TM edges and $N_{TM}/N_{Pt} = 2$ at the Pt edges, corresponding to chemically ordered NPs, allow us to quasiperfectly adjust the experimental measurements (Fig. 5). This result corroborates, on the NP assemblies, the observations performed in HRTEM.

Interestingly, the DW parameter deduced from fits is unusually large ($\approx 10^{-2}$ Å^2 mean square relative displacement) for the TM-TM, TM-Pt, and Pt-Pt bonds which is the signature of a significant dispersion of NN distances [64].

TABLE II. For each annealed sample, distances between NNs deduced from the EXAFS fits and apparent c/a ratios (see text).

Sample		d_{TMTM} (nm)	d_{TMPt} (nm)	d_{PtPt} (nm)	c/a
CoPt	Co edge	0.257	0.262		1.04 ± 0.02
	Pt edge		0.262	0.271	0.93 ± 0.02
FePt	Fe edge	0.263	0.263		1.00 ± 0.02
	Pt edge		0.263	0.270	0.95 ± 0.02

As shown in Table II, the TM-Pt distances are different from d_{TMTM} and d_{PtPt}, which are themselves different, contrary to the bulk crystal (where d_{TMTM} and d_{PtPt} are equal). Then two apparent c/a tetragonalization ratios can be inferred from these distances, assuming a face-centered tetragonal (fct) crystal structure: $(c/a)_{TM} = \sqrt{2(d_{TMPt}/d_{TMTM})^2 - 1}$ and $(c/a)_{Pt} = \sqrt{2(d_{TMPt}/d_{PtPt})^2 - 1}$. Here, $(c/a)_{TM}$ can thus be evaluated from distances around the TM atoms, while $(c/a)_{Pt}$ is calculated from distances around the Pt atoms (see Table II). In the bulk crystal, both approaches are the same, but in NPs, the values inferred from EXAFS measurements reflect the local environment around a given type of atom. The fact that there are two different apparent c/a ratios means that the perfect crystalline structure is perturbed [65,66].

Strikingly, the Co environment corresponds to an apparent tetragonalization opposite to the bulk ($c/a > 1$, remember that the c/a ratios in bulk $L1_0$ CoPt and FePt are almost similar and ≈ 0.97 [67]). For FePt, we also find a larger apparent c/a around Fe atoms ($c/a \simeq 1$) even if the difference between the values deduced from both absorption edges is smaller than in CoPt NPs. This shows that the atomic relaxation is more pronounced in CoPt than in FePt NPs: In other words, the atomic structure of small FePt clusters is closer to a bulk $L1_0$ crystal than for CoPt clusters. Let us emphasize that EXAFS measurements only probe the local environment and, despite that they bear the signature of chemical $L1_0$ order, they cannot discriminate between mono-$L1_0$ and multi-$L1_0$ NPs.

The different relaxation magnitude in CoPt and FePt NPs suggests that the different magnetic anisotropy properties identified in Sec. III could result from a local modification of the tetragonalization (c/a ratio). Some theoretical bulk calculations have already correlated the c/a ratio, the degree of chemical order, and the magnetic anisotropy energy [68–71]. It has been shown that a modification of the c/a ratio in a range like the one deduced from EXAFS (see Table II) only has a weak influence on the magnetic anisotropy.

We can then argue that the different local tetragonalization in CoPt vs FePt NPs does not seem to be the reason for the different magnetic behavior in both nanoalloys. To get a deeper understanding of the relaxation effects, we have performed first-principles calculations.

VI. STRUCTURAL RELAXATION CALCULATIONS

The calculations have been performed by using the Vienna *ab initio* Simulation Package [72,73] which implements the density functional theory of Hohenberg-Kohn-Sham on a periodic supercell and allows fully self-consistent unconstrained structural relaxations. It should be noted, however, that our goal cannot be to explain or reproduce the experimental EXAFS results in their full extent. In fact, the EXAFS experiment is performed on a very large variety of chemically ordered NPs [monodomain, multidomain, icosahedral, etc. (see Sec. II)] and therefore reflects only a mean value of the apparent tetragonalization which can be different for individual structures.

We have then performed a first-principles theoretical study of the structure of monodomain $L1_0$ CoPt and FePt particles. The assumed particle geometries are perfect truncated octahedra having 38, 201, and 586 atoms. The truncated octahedron

TABLE III. Average interatomic distances and apparent c/a ratios (see text) for relaxed $L1_0$ CoPt and FePt clusters having 586 atoms, as obtained from DFT calculations.

Sample		d_{TMTM} (nm)	d_{TMPt} (nm)	d_{PtPt} (nm)	c/a
CoPt	Co sites	0.264	0.264		1.00
	Pt sites		0.264	0.270	0.95
FePt	Fe sites	0.270	0.267		0.98
	Pt sites		0.267	0.273	0.96

is an equilibrium shape predicted by Wulff theory, and even if the actual structures of some particles may be different, we expect that the atomic relaxation mechanisms are robust enough to give insight into both mono-$L1_0$ and multi-$L1_0$ NPs. Moreover, the most intriguing magnetic feature concerns mono-$L1_0$ particles (which for CoPt seems to have a much lower anisotropy than for the bulk).

Table III compares the mean interatomic distances in chemically $L1_0$ ordered CoPt and FePt truncated octahedra with 586 atoms. The mean TM NN bonds are shorter than the Pt ones, leading to structural stress, and we find that a finite TM-Pt cluster can be more easily distorted by moving the TM atoms. This effect is particularly strong in the CoPt alloy (see Fig. 6). Following the EXAFS analysis, we can compute an apparent c/a, which is defined here around the two types of atoms by using the average NN TM-Pt and either Pt-Pt or TM-TM distances. This quantity is then a ratio of mean values, rather than a mean local tetragonalization.

The apparent c/a ratios at the TM sites are obviously different in both alloys, whereas the apparent c/a ratios at the Pt sites are almost the same. The relaxation effect is clearly less significant in FePt NPs. This feature is in agreement with the conclusions deduced from experimental EXAFS results. The apparent c/a ratio appears to be a simple tool to qualitatively
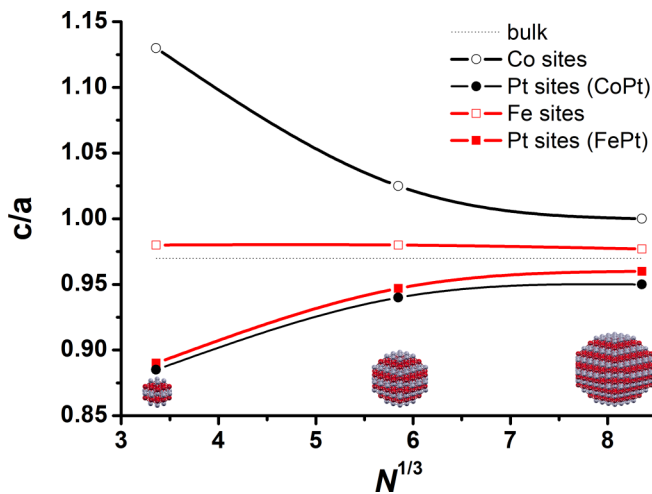

FIG. 6. Comparison between the apparent c/a ratios for the transition metal (TM) and Pt sites. N represents the number of atoms used to build perfect truncated octahedrons ($N^{1/3}$ periodicity). The lines are drawn to guide the eye. The dashed line represents the c/a ratio in the $L1_0$ bulk phase.
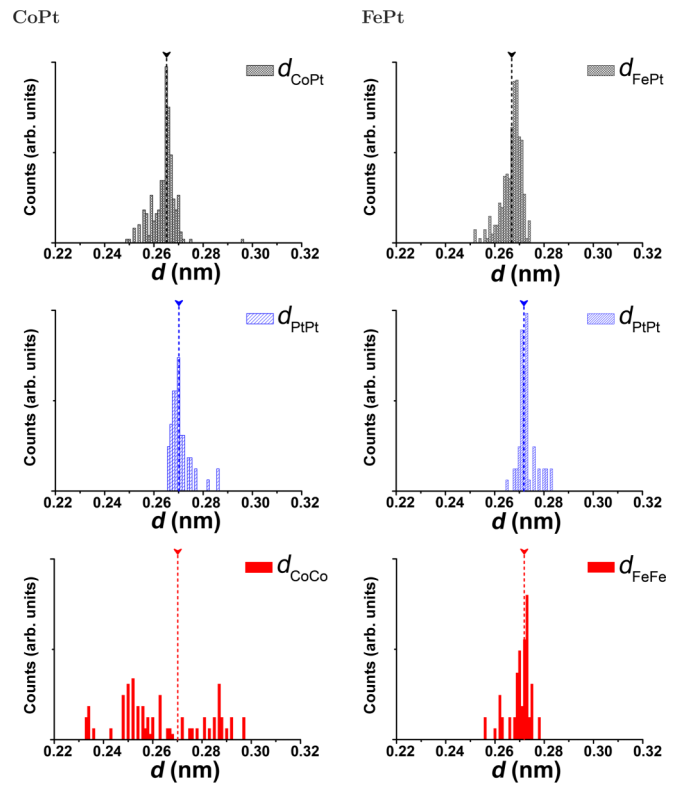

FIG. 7. Nearest-neighbor distances obtained from calculations on chemically ordered CoPt and FePt nanoparticles (586 atoms). The arrows represent distances in the $L1_0$ bulk alloys. To facilitate a clear comparison, the scales used are identical.

compare EXAFS results and theoretical investigations, but it does not reflect the full complexity associated with atomic relaxations in finite-sized clusters. It would be too simplistic to conclude that the relaxation only induces a different local tetragonalization in FePt and CoPt NPs. What is striking, more than the deviation from the bulk value, is the large magnitude of the apparent c/a difference between Co and Pt sites. This is the signature of a strong relaxation, especially for Co atoms, which means a significant breaking of the $L1_0$ crystal symmetry.

To go further, we plot in Fig. 7 all the NN distances calculated for clusters having 586 atoms. It becomes clear then, even if the mean distances are close to the bulk values for both nanoalloys (see Table III), that the distributions of the d_{CoCo} and d_{FeFe} are completely different. The standard deviation of d_{CoCo} is extremely large [$\sigma(d_{CoCo}) = 0.017$ nm], whereas for FePt NPs, the distributions of both d_{FeFe} and d_{PtPt} are narrow [$\sigma(d_{FeFe}) = 0.004$ nm]. In fact, this appears to be the major structural difference between both nanoalloys. Although the particles are chemically ordered, atomic relaxation induces an important crystallographic disorder, especially in the Co planes. The relaxed CoPt NP structure is far from a perfect crystal [65]. Comparatively, we find that, in FePt NPs, the behavior of Fe atoms is comparable with Pt atoms, with a moderate disordering.

This striking difference between CoPt and FePt NPs should be reflected in their magnetic properties. We can then infer that the reduced magnetic anisotropy in CoPt, where even

the presence of mono-$L1_0$ is not accompanied with a large anisotropy contribution, is due to the specific finite-sized relaxation and more precisely to the wide d_{CoCo} interatomic distance distribution. Following this idea, since the atomic relaxation is lower in $L1_0$ FePt NPs (narrower d_{FeFe} distribution), it allows us to explain why the anisotropy of mono-$L1_0$ particles is so large (in the MJ m^{-3} range). Additionally, it should be kept in mind that, for both FePt and CoPt, there are many different NP geometries. Particularly, there exist multi$L1_0$ particles which give a wide anisotropy distribution centered around a similar value ($\overline{K_1} \simeq 350$ kJ m^{-3}). Finally, a complete and systematic theoretical study of the magnetic properties in these relaxed structures needs to be done to fully understand the detailed mechanisms linking the atomic structure and the magnetic anisotropy. Such a numerical investigation is delicate and beyond the scope of this paper.

VII. CONCLUSIONS

The structure and magnetic properties of both chemically ordered CoPt and FePt NPs have been investigated. Although they are very similar for the bulk $L1_0$ phase, we find striking differences in terms of magnetic anisotropy. For FePt NPs, a strong anisotropy contribution ($K_1 = 1.1$ MJ m^{-3}) can be attributed to mono-$L1_0$ particles, whereas CoPt NPs exhibit a much reduced magnetic anisotropy ($K_1 = 330$ kJ m^{-3}), even if mono-$L1_0$ particles are also observed. From an application point of view, if the goal is to obtain a strong anisotropy, a strong switching field, and a high blocking temperature, then FePt appears to be preferable to CoPt.

EXAFS measurements have been used to determine the atomic structure of annealed CoPt and FePt NPs. We find that the NPs are chemically ordered but with different apparent tetragonalization ratios. DFT calculations on relaxed mono-$L1_0$ truncated octahedral clusters shed light on the finite-sized atomic relaxation effects: The $L1_0$ crystalline order is disturbed, especially in CoPt NPs where we find a wide d_{CoCo} interatomic distance distribution. This feature, which is absent in the case of FePt NPs, could explain the major anisotropy difference between both nanoalloys. Additional finite-sized effects, namely, the existence of numerous particle geometries with potential strain, defects, and surface disorder [74,75], may play a role in the magnetic anisotropy reduction compared with the bulk, as well as in the difference between FePt and CoPt alloys. Further progress requires a systematic and profound theoretical investigation to relate the magnetic properties to the detailed atomic structure.

[1] Z. Fan, M. Shelton, A. K. Singh, D. Senapati, S. A. Khan, and P. C. Ray, Multifunctional plasmonic shell-magnetic core nanoparticles for targeted diagnostics, isolation, and photothermal destruction of tumor cells, ACS Nano **6**, 1065 (2012).

[2] A. K. Gupta and M. Gupta, Synthesis and surface engineering of iron oxide nanoparticles for biomedical applications, Biomaterials **26**, 3995 (2005).

[3] T. A. Larson, J. Bankson, J. Aaron, and K. Sokolov, Hybrid plasmonic magnetic nanoparticles as molecular specific agents for MRI/optical imaging and photothermal therapy of cancer cells, Nanotechnology **18**, 325101 (2007).

[4] W.-R. Lee, M. G. Kim, J.-R. Choi, J.-I. Park, S. J. Ko, S. J. Oh, and J. Cheon, Redox-transmetalation process as a generalized synthetic strategy for core-shell magnetic nanoparticles, J. Am. Chem. Soc. **127**, 16090 (2005).

[5] A.-H. Lu, E. L. Salabas, and F. Schüth, Magnetic nanoparticles: Synthesis, protection, functionalization, and application, Angew. Chem., Int. Ed. **46**, 1222 (2007).

[6] D. M. Newman, M. L. Wears, M. Jollie, and D. Choo, Fabrication and characterization of nano-particulate PtCo media for ultra-high density perpendicular magnetic recording, Nanotechnology **18**, 205301 (2007).

[7] R. Sharma and C. J. Chen, Newer nanoparticles in hyperthermia treatment and thermometry, J. Nanopart. Res. **11**, 671 (2009).

[8] M. Shliomis and V. Stepanov, Frequency dependence and long time relaxation of the susceptibility of the magnetic fluids, J. Magn. Magn. Mater. **122**, 176 (1993).

[9] S. U. Son, Y. Jang, J. Park, H. B. Na, H. M. Park, H. J. Yun, J. Lee, and T. Hyeon, Designed synthesis of atom-economical Pd/Ni bimetallic nanoparticle-based catalysts for Sonogashira coupling reactions, J. Am. Chem. Soc. **126**, 5026 (2004).

[10] C. Xu, K. Xu, H. Gu, X. Zhong, Z. Guo, R. Zheng, X. Zhang, and B. Xu, Nitrilotriacetic acid-modified magnetic nanoparticles as a general agent to bind histidine-tagged proteins, J. Am. Chem. Soc. **126**, 3392 (2004).

[11] S. Sun, Monodisperse FePt nanoparticles and ferromagnetic FePt nanocrystal superlattices, Science **287**, 1989 (2000).

[12] Y. Chen, F. Yang, Y. Dai, W. Wang, and S. Chen, Ni@Pt coreshell nanoparticles: Synthesis, structural and electrochemical properties, J. Phys. Chem. C **112**, 1645 (2008).

[13] D. L. Huber, Synthesis, properties, and applications of iron nanoparticles, Small **1**, 482 (2005).

[14] A. Tamion, M. Hillenkamp, A. Hillion, V. A. Maraloiu, I. D. Vlaicu, M. Stefan, D. Ghica, H. Rositi, F. Chauveau, M.-G. Blanchin *et al.*, Ferritin surplus in mouse spleen 14 months after intravenous injection of iron oxide nanoparticles at clinical dose, Nano Res. **9**, 2398 (2016).

[15] E. Wohlfarth, The temperature dependence of the magnetic susceptibility of spin glasses, Phys. Lett. A **70**, 489 (1979).

[16] P. Andreazza, V. Pierron-Bohnes, F. Tournus, C. Andreazza-Vignolle, and V. Dupuis, Structure and order in cobalt/platinum-type nanoalloys: From thin films to supported clusters, Surf. Sci. Rep. **70**, 188 (2015).

[17] K. Barmak, J. Kim, L. H. Lewis, K. R. Coffey, M. F. Toney, A. J. Kellock, and J.-U. Thiele, On the relationship of

magnetocrystalline anisotropy and stoichiometry in epitaxial L10 CoPt (001) and FePt (001) thin films, J. Appl. Phys. **98**, 033904 (2005).

[18] A. C. C. Yu, M. Mizuno, Y. Sasaki, M. Inoue, H. Kondo, I. Ohta, D. Djayaprawira, and M. Takahashi, Fabrication of monodispersive FePt nanoparticle films stabilized on rigid substrates, Appl. Phys. Lett. **82**, 4352 (2003).

[19] M. Yu, Y. Liu, and D. J. Sellmyer, Nanostructure and magnetic properties of composite CoPt : C films for extremely high-density recording, J. Appl. Phys. **87**, 6959 (2000).

[20] Y. Xu, Z. Sun, Y. Qiang, and D. Sellmyer, Preparation and magnetic properties of CoPt and CoPt : Ag nanocluster films, J. Magn. Magn. Mater. **266**, 164 (2003).

[21] M. S. Wellons, Z. Gai, J. Shen, J. Bentley, J. E. Wittig, and C. M. Lukehart, Synthesis of $L1_0$ ferromagnetic CoPt nanopowders using a single-source molecular precursor and water-soluble support, J. Mater. Chem. C **1**, 5976 (2013).

[22] T. Seto, K. Koga, H. Akinaga, F. Takano, T. Orii, and M. Hirasawa, Laser ablation synthesis of monodispersed magnetic alloy nanoparticles, J. Nanopart. Res. **8**, 371 (2006).

[23] J. H. Kim, J. Kim, N. Oh, Y.-H. Kim, C. K. Kim, C. S. Yoon, and S. Jin, Monolayer CoPt magnetic nanoparticle array using multiple thin film depositions, Appl. Phys. Lett. **90**, 023117 (2007).

[24] C. N. Chinnasamy, B. Jeyadevan, K. Shinoda, and K. Tohji, Polyol-process-derived CoPt nanoparticles: Structural and magnetic properties, J. Appl. Phys. **93**, 7583 (2003).

[25] D. Alloyeau, C. Langlois, C. Ricolleau, Y. Le Bouar, and A. Loiseau, A TEM *in situ* experiment as a guideline for the synthesis of as-grown ordered CoPt nanoparticles, Nanotechnology **18**, 375301 (2007).

[26] M. Pellarin, E. Cottancin, J. Lermé, J. L. Vialle, J. P. Wolf, M. Broyer, V. Paillard, V. Dupuis, A. Perez, and J. P. Perez, High-efficiency cluster laser vaporization sources based on Ti : Sapphire lasers, Chem. Phys. Lett. **224**, 338 (1994).

[27] A. Perez, P. Melinon, V. Dupuis, L. Bardotti, B. Masenelli, F. Tournus, B. Prevel, J. Tuaillon-Combes, E. Bernstein, and A. Tamion, Functional nanostructures from clusters, Int. J. Nanotechnol. **7**, 523 (2010).

[28] F. Tournus, A. Tamion, N. Blanc, A. Hannour, L. Bardotti, B. Prével, P. Ohresser, E. Bonet, T. Epicier, and V. Dupuis, Evidence of $L1_0$ chemical order in CoPt nanoclusters: Direct observation and magnetic signature, Phys. Rev. B **77**, 144411 (2008).

[29] F. Tournus, N. Blanc, A. Tamion, M. Hillenkamp, and V. Dupuis, Dispersion of magnetic anisotropy in size-selected CoPt clusters, Phys. Rev. B **81**, 220405(R) (2010).

[30] A. Hillion, A. Cavallin, S. Vlaic, A. Tamion, F. Tournus, G. Khadra, J. Dreiser, C. Piamonteze, F. Nolting, S. Rusponi *et al.*, Low Temperature Ferromagnetism in Chemically Ordered FeRh Nanocrystals, Phys. Rev. Lett. **110**, 087207 (2013).

[31] V. Dupuis, G. Khadra, S. Linas, A. Hillion, L. Gragnaniello, A. Tamion, J. Tuaillon-Combes, L. Bardotti, F. Tournus, E. Otero *et al.*, Magnetic moments in chemically ordered mass-selected CoPt and FePt clusters, J. Magn. Magn. Mater. **383**, 73 (2015).

[32] C.-b. Rong, D. Li, V. Nandwana, N. Poudyal, Y. Ding, Z. L. Wang, H. Zeng, and J. P. Liu, Size-dependent chemical and magnetic ordering in $L1_0$-FePt nanoparticles, Adv. Mater. **18**, 2984 (2006).

[33] F. Tournus, K. Sato, T. Epicier, T. J. Konno, and V. Dupuis, Multi-$L1_0$ Domain CoPt and FePt Nanoparticles Revealed by Electron Microscopy, Phys. Rev. Lett. **110**, 055501 (2013).

[34] P. Capiod, L. Bardotti, A. Tamion, O. Boisron, C. Albin, V. Dupuis, G. Renaud, P. Ohresser, and F. Tournus, Elaboration of Nanomagnet Arrays: Organization and Magnetic Properties of Mass-Selected FePt Nanoparticles Deposited on Epitaxially Grown Graphene on Ir(111), Phys. Rev. Lett. **122**, 106802 (2019).

[35] R. Alayan, L. Arnaud, A. Bourgey, M. Broyer, E. Cottancin, J. R. Huntzinger, J. Lermé, J. L. Vialle, M. Pellarin, and G. Guiraud, Application of a static quadrupole deviator to the deposition of size-selected cluster ions from a laser vaporization source, Rev. Sci. Instrum. **75**, 2461 (2004).

[36] D. Tainoff, L. Bardotti, F. Tournus, G. Guiraud, O. Boisron, and P. Mélinon, Self-organization of size-selected bare platinum nanoclusters: Toward ultra-dense catalytic systems, J. Phys. Chem. C **112**, 6842 (2008).

[37] E. P. Wohlfarth, Relations between different modes of acquisition of the remanent magnetization of ferromagnetic particles, J. Appl. Phys. **29**, 595 (1958).

[38] O. Henkel, Remanenzverhalten und Wechselwirkungen in hart-magnetischen Teilchenkollektiven, Phys. Status Solidi B **7**, 919 (1964).

[39] F. Tournus, Modelling of isothermal remanence magnetisation curves for an assembly of macrospins, J. Magn. Magn. Mater. **375**, 194 (2015).

[40] F. Wehland, A. Stancu, P. Rochette, M. Dekkers, and E. Appel, Experimental evaluation of magnetic interaction in pyrrhotite bearing samples, Phys. Earth Planet. Inter. **153**, 181 (2005).

[41] J. M. Martínez Huerta, J. De La Torre Medina, L. Piraux, and A. Encinas, Self consistent measurement and removal of the dipolar interaction field in magnetic particle assemblies and the determination of their intrinsic switching field distribution, J. Appl. Phys. **111**, 083914 (2012).

[42] A. Hillion, A. Tamion, F. Tournus, C. Albin, and V. Dupuis, From vanishing interaction to superferromagnetic dimerization: Experimental determination of interaction lengths for embedded Co clusters, Phys. Rev. B **95**, 134446 (2017).

[43] K. Sato, T. J. Konno, and Y. Hirotsu, Atomic structure imaging of $L1_0$-type FePd nanoparticles by spherical aberration corrected high-resolution transmission electron microscopy, J. Appl. Phys. **105**, 034308 (2009).

[44] N. Blanc, F. Tournus, V. Dupuis, and T. Epicier, Measuring the $L1_0$ chemical order parameter of a single CoPt nanoparticle smaller than 4 nm, Phys. Rev. B **83**, 092403 (2011).

[45] P. Entel, M. Gruner, G. Rollmann, A. Hucht, S. Sahoo, A. Zayak, H. Herper, and A. Dannenberg, First-principles investigations of multimetallic transition metal clusters, Philos. Mag. **88**, 2725 (2008).

[46] G. Rossi, R. Ferrando, and C. Mottet, Structure and chemical ordering in CoPt nanoalloys, Faraday Discuss. **138**, 193 (2008).

[47] P. Andreazza, C. Mottet, C. Andreazza-Vignolle, J. Penuelas, H. C. N. Tolentino, M. De Santis, R. Felici, and N. Bouet, Probing nanoscale structural and order/disorder phase transitions of supported Co-Pt clusters under annealing, Phys. Rev. B **82**, 155453 (2010).

[48] A. Tamion, M. Hillenkamp, F. Tournus, E. Bonet, and V. Dupuis, Accurate determination of the magnetic anisotropy in cluster-assembled nanostructures, Appl. Phys. Lett. **95**, 062503 (2009).

[49] A. Tamion, E. Bonet, F. Tournus, C. Raufast, A. Hillion, O. Gaier, and V. Dupuis, Efficient hysteresis loop simulations of nanoparticle assemblies beyond the uniaxial anisotropy, Phys. Rev. B **85**, 134430 (2012).

[50] A. Hillion, A. Tamion, F. Tournus, O. Gaier, E. Bonet, C. Albin, and V. Dupuis, Advanced magnetic anisotropy determination through isothermal remanent magnetization of nanoparticles, Phys. Rev. B **88**, 094419 (2013).

[51] S. Oyarzún, A. Tamion, F. Tournus, V. Dupuis, and M. Hillenkamp, Size effects in the magnetic anisotropy of embedded cobalt nanoparticles: From shape to surface, Sci. Rep. **5**, 14749 (2015).

[52] A. Thiaville, Coherent rotation of magnetization in three dimensions: A geometrical approach, Phys. Rev. B **61**, 12221 (2000).

[53] A. Tamion, C. Raufast, M. Hillenkamp, E. Bonet, J. Jouanguy, B. Canut, E. Bernstein, O. Boisron, W. Wernsdorfer, and V. Dupuis, Magnetic anisotropy of embedded Co nanoparticles: Influence of the surrounding matrix, Phys. Rev. B **81**, 144403 (2010).

[54] M. Jamet, W. Wernsdorfer, C. Thirion, D. Mailly, V. Dupuis, P. Mélinon, and A. Pérez, Magnetic Anisotropy of a Single Cobalt Nanocluster, Phys. Rev. Lett. **86**, 4676 (2001).

[55] M. Jamet, W. Wernsdorfer, C. Thirion, V. Dupuis, P. Mélinon, A. Pérez, and D. Mailly, Magnetic anisotropy in single clusters, Phys. Rev. B **69**, 024401 (2004).

[56] Y. Xie and J. A. Blackman, Magnetic anisotropy of nanoscale cobalt particles, J. Phys.: Condens. Matter **16**, 3163 (2004).

[57] V. Dupuis, N. Blanc, L. E. Diaz-Sanchez, A. Hillion, A. Tamion, F. Tournus, G. M. Pastor, A. Rogalev, and F. Wilhelm, Finite size effects on structure and magnetism in mass-selected CoPt nanoparticles, Eur. Phys. J. D **67**, 25 (2013).

[58] S. Rohart, F. Tournus, and V. Dupuis, Chemical order and size effects on the magnetic anisotropy of FePt and CoPt nanoparticles, arXiv:1105.6292 (2011).

[59] Z. Liu and G. Wang, Shape-dependent surface magnetism of Co-Pt and Fe-Pt nanoparticles from first principles, Phys. Rev. B **96**, 224412 (2017).

[60] R. Cuadrado and R. W. Chantrell, Electronic and magnetic properties of bimetallic *L*1₀ cuboctahedral clusters by means of fully relativistic density-functional-based calculations, Phys. Rev. B **86**, 224415 (2012).

[61] O. Proux, V. Nassif, A. Prat, O. Ulrich, E. Lahera, X. Biquard, J.-J. Menthonnex, and J.-L. Hazemann, Feedback system of a liquid-nitrogen-cooled double-crystal monochromator: Design and performances, J. Synchrotron Radiat. **13**, 59 (2006).

[62] J. Goulon, A. Rogalev, G. Goujon, C. Gauthier, E. Moguiline, A. Solé, S. Feite, F. Wilhelm, N. Jaouen, C. Goulon-Ginet *et al.*, Advanced detection systems for x-ray fluorescence excitation spectroscopy, J. Synchrotron Radiat. **12**, 57 (2005).

[63] B. Ravel and M. Newville, ATHENA, ARTEMIS, HEPHAESTUS: Data analysis for x-ray absorption spectroscopy using IFEFFIT, J. Synchrotron Radiat. **12**, 537 (2005).

[64] G. Greco, A. Witkowska, E. Principi, M. Minicucci, and A. Di Cicco, Local structural and chemical ordering of nanosized Pt $3 \pm \delta$ Co probed by multiple-scattering x-ray absorption spectroscopy, Phys. Rev. B **83**, 134103 (2011).

[65] N. Blanc, L. E. Díaz-Sánchez, A. Y. Ramos, F. Tournus, H. C. N. Tolentino, M. De Santis, O. Proux, A. Tamion, J. Tuaillon-Combes, L. Bardotti *et al.*, Element-specific quantitative determination of the local atomic order in CoPt alloy nanoparticles: Experiment and theory, Phys. Rev. B **87**, 155412 (2013).

[66] M. Hennes, E. Fonda, N. Casaretto, J. Buchwald, X. Weng, G. Patriarche, D. Demaille, Y. Zheng, and F. Vidal, Structural, vibrational, and magnetic properties of self-assembled CoPt nanoalloys embedded in SrTiO₃, Phys. Rev. Mater. **4**, 126001 (2020).

[67] A. Menshikov, T. Tarnóczi, and E. Krén, Magnetic structure of Ordered FePt and Fe₃Pt alloys, Phys. Status Solidi A **28**, K85 (1975).

[68] J. B. Staunton, S. Ostanin, S. S. A. Razee, B. Gyorffy, L. Szunyogh, B. Ginatempo, and E. Bruno, Long-range chemical order effects upon the magnetic anisotropy of FePt alloys from an *ab initio* electronic structure theory, J. Phys.: Condens. Matter **16**, S5623 (2004).

[69] T. Burkert, O. Eriksson, S. I. Simak, A. V. Ruban, B. Sanyal, L. Nordström, and J. M. Wills, Magnetic anisotropy of *L*1₀ FePt and Fe₁₋ₓMnₓPt, Phys. Rev. B **71**, 134411 (2005).

[70] P. V. Lukashev, N. Horrell, and R. F. Sabirianov, Tailoring magnetocrystalline anisotropy of FePt by external strain, J. Appl. Phys. **111**, 07A318 (2012).

[71] Y. Yang, C.-C. Chen, M. C. Scott, C. Ophus, R. Xu, A. Pryor, L. Wu, F. Sun, W. Theis, J. Zhou *et al.*, Deciphering chemical order/disorder and material properties at the single-atom level, Nature (London) **542**, 75 (2017).

[72] G. Kresse and J. Furthmuller, Efficient iterative schemes for *ab initio* total-energy calculations using a plane-wave basis set, Phys. Rev. B **54**, 11169 (1996).

[73] G. Kresse and D. Joubert, From ultrasoft pseudopotentials to the projector augmented-wave method, Phys. Rev. B **59**, 1758 (1999).

[74] A. Front, B. Legrand, G. Tréglia, and C. Mottet, Bidimensional phases in Co-Pt surface alloys: A theoretical study of ordering and surface segregation, Surf. Sci. **679**, 128 (2019).

[75] A. Front and C. Mottet, Ordering frustration in large-scale Co-Pt nanoalloys, J. Phys. Chem. C **125**, 16358 (2021).